PROPOSAL FOR A NOVEL PEROVSKITE SOLAR CELL BASE ON $BaZrS_3$ WITH OPTIMIZED ELECTRON AND HOLE TRANSPORT LAYER USING SCAPS-1D

Shreyus Goutham Kumar[1], Suraj N[2], Anmol Pramod[2], Prashanth C R[3], Gajanan V Honnavar[4]

Article History: **Received:** 25.05.2023 **Revised:** 15.06.2023 **Accepted:** 02.08.2023

Abstract:

Perovskite solar cells have made impressive strides in recent years, with efficiency rising quickly from reports of around 3% in 2009 to over 25% now. Chalcogenides are one of the main compounds applied as absorbers of highly efficient photovoltaic devices based on thin-film technology. This paper analyses the energy conversion in a Chalcogenide Perovskite Solar Cell with $BaZrS_3$ as the absorber layer. The effects of different Electron and Hole transport layers are thoroughly discussed. According to our analysis, ZnO and CuSbS2 are the best ETL and HTL layers respectively. The thickness and defect density of the absorber, ETL and HTL has been optimized to get the highest PCE. The density of defects in the interface layers has also been optimized. The final proposed structure-FTO/ZnO/$BaZrS_3$/$CuSbS_2$/back-contact has a PCE of 26.54%.

Keywords: Chalcogenide, Perovskite, solar-cell, numerical simulation, material optimization, SCAPS 1D

[1]Dept. of Electronics and Communication, PES University, EC Campus, Hosur Road, Near Electronic City, Bangalore 560100, India and Research Scholar in Dept on ETE, Dr. AIT, Affiliated to VTU, Belagavi, India.

[2]Dept. of Electronics and Communication, PES University, EC Campus, Hosur Road, Near Electronic City, Bangalore 560100, India

[3]Dept. of Electronics and Telecommunication, Dr. Ambedkar Institute of Technology, Affiliated to VTU, Bengaluru, Karnataka 560056, India

[4]Dept. of Science and Humanities, PES University, EC Campus, Hosur Road, Near Electronic City, Bangalore 560100, India

DOI: 10.48047/ecb/2023.12.10.728

1. Introduction

Solar cells are the source of clean and green energy harvested from the sun. The need for green energy is more important now than ever, following the natural calamity that are related to global warming. The rapidly depleting supply of fossil fuels and their detrimental impact on the environment have caused the globe to become more interested in the advancement of renewable and environmentally friendly energy sources. Due to this, much effort was put into creating sophisticated photovoltaic technology to lower processing costs and boost power conversion efficiency (PCE). Perovskite Solar Cells (PSC) are a transpiring photovoltaic technology having a perovskite-structured compound as absorber layer. These cells have shown the capability for high performance at a low cost of production. These materials provide excellent light ingestion, charge-transporter mobilities, life, and adaptability for the industries [1] . The PSCs have shown exceptional progress in recent times with rapid increase in conversion efficiency of 3% to 25% in the past 15 years. Pb-based PSC devices have been the subject of numerous investigations over the past ten years, and their efficiency as light-absorbing materials is currently 25.2 % [2] – [4].On the other hand, commercialization of these materials is constrained because of the toxicity of lead in the material and instability problems brought on by applied electric field, light , heat or moisture which motivates the search for substitute solar cell materials. Consequently, non-lead-based PSCs are becoming more popular [5].

Chalcogenide perovskites (CPs) has newly surfaced as a potential environmentally safe, and a semiconductor material which is not hazardous. Therefore, it has received widespread interest because of its wonderful optoelectronic properties [6]. The general formula for the CPs material is ABX_3, where A denotes group II cations (such as Sr^{2+}, Ca^{2+}, and Ba^{2+}), B denotes group IV transition metals (such as Zr^{4+}, Ti^{4+}, and Hf^{4+}), and X denotes chalcogen anions (such as S^{2-} and Se^{2-}), respectively. Due to their higher environmental stability and Pb-free nature, barium zirconium sulphide ($BaZrS_3$) CPs have undergone the most experimental research. [7] – [10]. Additionally, among other distinctive characteristics, it has a significant absorption coefficient (>105 cm^{-1}), great carrier mobility, and good defect tolerance [8]. $BaZrS_3$ enables a more accessible collection of photo-generated carriers because of the significant band-edge absorption of and the low light penetration depth (~100 nm). [11]. $BaZrS_3$ CPs have a band gap between 1.7eV and 1.9 eV, which is greater than the optimum band gap needed for single-junction devices [12]. According to a few studies $BaZrS_3$ can be tuned to have a bandgap of 1.47 eV or 1.51 eV by alloying it with Ti [13]. However, present work mainly focuses on bringing the right combination of ETL and HTL along with $BaZrS_3$ to get optimum efficiency.

The simulations of the devices are based on the solar cell's one-dimensional structure. The 1-D Solar Cell Capacitance Simulator (SCAPS), which was created at the University of Gent by Burgelman et.al to model different types of solar cells, is used to evaluate the performance of these devices [14]. Fundamental semiconductor equations like the continuity and Poisson equations with the drift-diffusion approximation can be solved using the SCAPS software. Current-voltage curve and quantum efficiency, and other electrical characteristics of solar cells are simulated. Although it was initially intended to analyze CdTe or CIGS type solar cells, SCAPS also works well for such structures, even when the parameters are substantially different from those of CIGS or CdTe [14]. These days, it has been successfully used in bulk heterojunction solar cell architectures, perovskite solar cells, c-Si solar cells, and CZTS solar cells. (Latest version: SCAPS Basic Manual.pdf). Additionally, many organizations have already built the new device configuration using new absorber materials using the SCAPS program. The simulations are obviously helpful to those in the solar cell community because they are significantly more dependable than the experimental results.

The novelty of this article is to bring in the right combination of ETL and HTL along with BaZrS3 to get optimum efficiency, and to improve the efficiency of the C-PSC, the electrical

performance of the device was calculated in order to optimize the physical properties.

Organization of the paper: Section 1 provides background information on perovskite solar cells as well as a brief description of the proposed work's objectives. Section 2 explains the materials and methodology utilized for the proposed PSC, Section 3 examines the analysis results, Section 4 discusses the proposed structure, and Section 5 has the conclusion.

2. Materials and Methodology

A. Structure of the device and input data

This paper mainly focuses on the chalcogenide perovskite $BaZrS_3$ as an absorber layer. The PSC's architecture, which consists of FTO/ETL/$BaZrS_3$/HTL, is shown in Fig.1. The transparent conducting oxide (TCO) in the structure is fluorine-doped tin oxide (FTO), whereas the absorber layer is $BaZrS_3$.The HTL layer, is p-type and the ETL layer is n-type. The absorber layer has a bandgap of 1.9eV and an electron affinity of 4.1eV. The band gap of $BaZrS_3$ ranges from 1.7 to 1.9 eV, and when the band gap is optimized 1.7 eV the PCE of the device improved so we selected $BaZrS_3$ with a bandgap of 1.7 eV for further optimization of the device. The band gap of 1.7 eV has been validated experimentally in [15]. The electron and hole mobility has also been validated in [16] Table I shows the physical parameters of the PSC layers. Using the SCAPS 1D tools, we analyze the electrical properties of the perovskite structures. The model is simulated using AM 1.5G light spectrum with a power of 100 mW/cm^2 at 300K. The reference Perovskite Solar Cell (FTO/TiO_2/$BaZrS_3$/Cu_2O/Au) [17] used as a baseline in this investigation is shown in Fig. 1, as having the following chemical composition. The transparent conducting oxide in this structure is a fluorine-doped tin oxide (FTO), and the absorber layer is Barium Zirconium Sulphide ($BaZrS_3$). The Optimized PSC in the reference structure has a PCE of 12.42%.

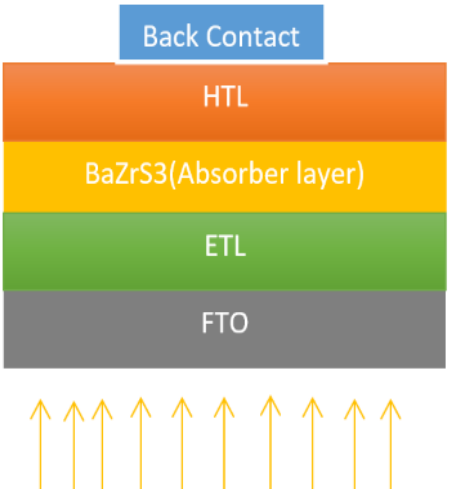

Fig. 1. C-PSC device configuration.

The approach employed in the study to improve the Chalcogenide-based PSC device is listed below. An ETL that successfully transports absorber layer's electrons to the appropriate contact is first chosen. Then, an HTL was selected to pass a significant amount of current efficiently from the

absorber layer to the relevant contacts in the cell. The optimal interface layer defect density is found, followed by optimizing the absorber layer thickness. To design the structure, we begin by taking TiO_2 and Spiro-OMeTAD as the ETL and HTL Material respectively. The absorber ($BaZrS_3$) layer is tested with several ETL and HTL materials. The material that improves the cell performance the maximum is chosen. As interface layers play a significant role in the capture of electrons and holes, we also investigate their impact when placed in between absorber layer and the charge transport layers. Perovskite/HTL interface (IL1) is situated between the absorber layer and the HTL, whereas the ETL/perovskite interface (IL2) is situated between ETL and the $BaZrS_3$ absorber layer. From the previous theoretical and experimental analysis, all physical and electrical parameters required for the materials previously chosen were obtained, and they are all displayed in Table I

.

Table I Physical properties used as basis for simulation with their respective references

Parameters	**FTO**	**TiO_2**	**$MASnBr_3$**	**Spiro-OMeTAD**
Thickness (nm)	500	100	500	200
E_g (eV)	3.5	3.2	1.3	3.0
χ (eV)	4.0	3.9	4.170	2.45
ϵ_r	9.0	9.0	10	3.0
N_c (cm^{-3})	$1x10^{19}$	$1x10^{21}$	$2.2x10^{18}$	$1x10^{19}$
N_v (cm^{-3})	$1x10^{19}$	$2x10^{20}$	$1.8x10^{18}$	$1x10^{19}$
μ_n (cm^2/Vs)	100	20	1.6	0.0002
μ_p (cm^2/Vs)	25	10	1.6	0.0002
N_d (cm^{-3})	$2x10^{19}$	$1x10^{17}$	$1x10^{13}$	0
N_a (cm^{-3})	0	0	$1x10^{13}$	$1x10^{18}$
N_t (cm^{-3})	$1x10^{14}$	$1x10^{15}$	$1x10^{15}$	$1x10^{15}$

Where Eg is bandgap, χ is electron affinity, ε_r is dielectric permittivity, Nc is Conduction Band effective density of states ,Nv is Valance Band effective density of states, μ_e is electron mobility, μ_h is hole mobility, N_D is shallow uniform donor density, N_A shallow uniform acceptor density and N_t is total defect density. Table II and Table III shows the physical properties of ETL and HTL layers respectively. Different ETL materials whose parameters are taken from [18] – [23] are listed in Table II.

Table II Physical characteristics of the various ETL layers with their respective references.

Parameters	**PCBM**[19,20]	**C_{60}**[21]	**CdS**[22]	**ZnO**[18]	**LBSO**[23]	**IGZO**[18,23]
Thickness(nm)	100	100	100	100	100	100
E_g (eV)	2	1.7	2.4	3.3	3.12	3.050
χ (eV)	3.9	3.9	4.2	4.1	4.4	4.16
ϵ_r	3.9	4.2	10	9	22	10.001
N_c (cm^{-3})	2.5×10^{21}	8×10^{19}	2.2×10^{18}	4×10^{18}	1.8×10^{20}	5×10^{18}
N_v (cm^{-3})	2.5×10^{19}	8×10^{19}	1.8×10^{18}	1×10^{19}	1.8×10^{20}	5×10^{18}
μ_e (cm^2/Vs)	0.2	0.08	100	100	0.69	15
μ_h (cm^2/Vs)	0.2	0.0035	25	50	0.69	0.1
N_d (cm^{-3})	2.93×10^{17}	2×10^{18}	1×10^{17}	1×10^{18}	2×10^{21}	1×10^{18}
N_a (cm^{-3})	0	0	0	1×10^{5}	0	0
N_t (cm^{-3})	1×10^{15}	1×10^{15}	1×10^{15}	1×10^{15}	1×10^{15}	1×10^{15}

Different HTL materials whose parameters are taken from [24] – [32] are listed in Table III. The thickness of HTL is kept fixed at 200nm for our analysis.

Table III Physical characteristics of the various HTL layers with their respective references

Parameters	**$CuSbS_2$**[24,31]	**CuI** [25,32]	**CuSCN**[26,27]	**Cu_2O** [28]	**P_3HT** [29]	**NiO**[30]
Eg (eV)	1.580	2.980	3.4	2.17	1.85	3.8
χ (eV)	4.2	2.1	1.9	3.2	3.1	1.46
ϵr	14.6	6.5	10	7.11	3.4	11.7
Nc (cm^{-3})	2×10^{18}	2.8×10^{19}	1.7×10^{19}	2.02×10^{18}	1×10^{22}	2.8×10^{19}
Nv (cm^{-3})	1×10^{19}	1×10^{19}	2.5×10^{21}	1.1×10^{19}	1×10^{22}	1×10^{19}
μ_e (cm^2/Vs)	49	0.00017	0.00015	200	0.0001	2.8
μ_h (cm^2/Vs)	49	0.0002	0.1	80	0.001	2.8
Nd (cm^{-3})	0	0	0	0	0	0
Na (cm^{-3})	1.38×10^{18}	1×10^{18}	1×10^{18}	1×10^{18}	3.1×10^{13}	1×10^{18}
Nt (cm^{-3})	1×10^{15}	1×10^{15}	1×10^{15}	1×10^{15}	1×10^{15}	1×10^{15}

Table IV tabulates the values of parameters for the interface of the perovskite layer, the HTL layer, and the ETL layer. The quantum efficiency (QE), fill factor (FF), Jsc-V characteristics and power conversion efficiency (PCE) are used to measure the solar cell's electrical performance. We are choosing neutral defect to avoid recombination.

Table IV Physical characteristics for interface of perovskite/HTL and perovskite/ETL.

Parameters	**HTL/C-perovskite interface**	**ETL/C-perovskite interface**
Defect type	Neutral	Neutral
Capture cross section electrons[cm^2]	NA	1×10^{-19}
Capture cross section holes[cm^2]	1×10^{-19}	NA
Reference of defect energy level	Above the highest eV	Above the highest eV
Energy with respect to reference[eV]	0.06	0.06
Total density[cm^{-2}]	1×10^{-10}	1×10^{-10}

B. Numerical Methods

In general, SCAPS 1D solves the four equations given below in Equations 1 to 4 which represent the photovoltaic equations for hole and electron carrier density independently [36].

1) Poisson equation:

$$\frac{d^2\varphi(x)}{\mathrm{d}x^2} = \frac{\mathrm{e}}{\epsilon_0 \in r}(p(x) - n(x) + N_D - N_A + \rho_p - \rho_n \quad (1)$$

Where N_D is the shallow donor impurity density and N_A is the shallow acceptor impurity density, e is the electronic charge, φ is the electrostatic potential, ε_0 is the free space permittivity, ε_r is the relative permittivity, and the hole and electron densities as a function of x (where x is direction of charge flow) are indicated by p(x) and n(x), respectively, while n is the electron density distribution and p is the hole density distribution.

2) Continuity equation:

$$\frac{\mathrm{d}J_n}{\mathrm{d}x} = G - R$$
$$\frac{dJ_p}{dx} = G - R \quad (2)$$

Where the current density of electron is Jn, the current density of hole is Jp, while the generation and recombination rates are G and R respectively.

3) Charge transport equation:

$$J_n = D_n\frac{dn}{dx} + \mu_n n\frac{d\varphi}{dx}$$
$$J_p = D_p\frac{dp}{dx} + \mu_p p\frac{d\varphi}{dx} \quad (3)$$

Where the electron mobility is denoted by μ_n, hole mobility is denoted by μ_p, electron diffusion coefficient and hole diffusion coefficients are D_n and D_p respectively.

4) Absorption coefficient equation:

$$\alpha(\lambda) = \left(A + \frac{B}{hv}\right)\sqrt{hv - E_g} \quad (4)$$

Where A and B are constants, h is the Plank constant, E_g is the absorber layer's band gap and v is photon frequency.

The simulation's output includes open circuit voltage (Voc) of 14.761 V, current density (Jsc) of 14.144 mA cm^2, FF of 77.53%, and efficiency of 16.19%.

3. Results and Discussions

A. Selection of ETL for C-PSC Device

The purpose of the electron transport layer is to transport electrons generated in the absorber layer due to splitting sunlight into electron-hole pairs to the PSC's front contact. Additionally, it prevents the holes from reaching the front contact by passing through the absorber layer. So, in order to choose the best ETL, we investigated the current density, Open-circuit voltage, and efficiency outcomes of several different ETLs with Spiro-OMeTAD as HTL.ETLs such as C_{60}, ZnO, PCBM, IGZO, CdS and LBSO are compared. Fig. 2. Illustrates effects of various ETL on the PSC. Physical parameters used in the simulation are given in Table II. Table V's results show that CdS

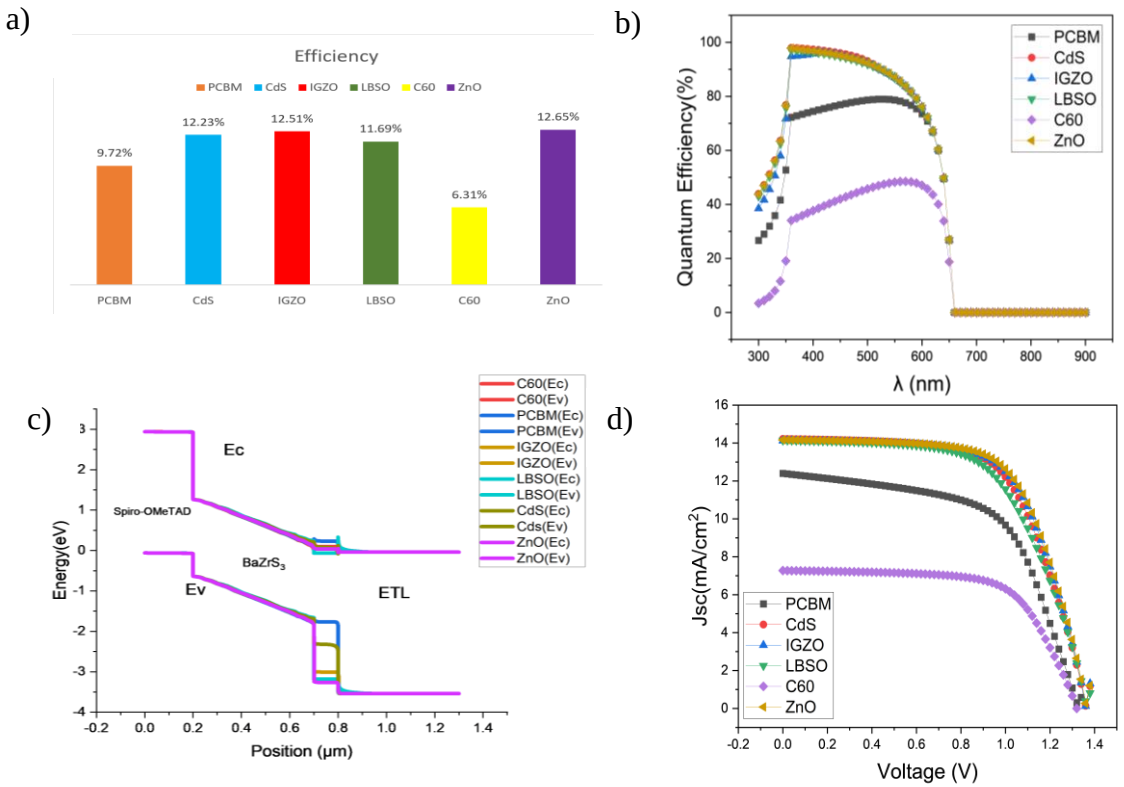

Fig. 2. Plot of different ETL on C-PSC: a) efficiency of C-PSC, b) Quantum Efficiency, c) Energy band diagram of all HTL, and d) J_{sc}–V characteristics.

Physical parameters used in the simulation are given in Table II. Table V's results show that CdS produced the maximum current density of 14.21mA/cm^2 whereas LBSO produced the highest open-circuit voltage (1.366 V). The only electron transport layers that outperform other ETLs with an efficiency of over 12.5% are IGZO and ZnO. From Fig. 2, it is possible to deduce the cause of the improvement in electrical performance. We select ZnO as the ideal layer for ETL since it has the highest PCE.

Table V Impact of different ETL on C-PSC device.

ETL	V_{oc}[V]	J_{sc} [mA cm^{-2}]	FF [%]	PCE [%]
PCBM	1.327	12.39	59.05	9.72
CdS	1.361	14.21	63.15	12.23
IGZO	1.361	14.12	65.05	12.51
LBSO	1.366	14.14	60.46	11.69
C_{60}	1.320	7.27	65.18	6.31
ZnO	1.363	14.16	65.45	12.65

B. Selection of HTL for C-PSC Device

In a solar cell, the hole transport layer (HTL) is a layer of material that helps to transport positive charges, or holes, from the -absorber layer to the electrical contact on the solar cell. One of the main purposes of the HTL is to improve the overall efficiency of the solar cell by reducing the recombination of holes and electrons, which can occur at the interface between the light-absorbing layer and the electrical contact. If holes and electrons recombine at this interface, they will not be able to contribute to the current generated by the solar cell, and the efficiency of the cell will be reduced. By providing a path for the holes to travel to the electrical contact, the HTL helps to prevent this recombination and improve the efficiency of the solar cell. After selecting the ETL material i.e., ZnO, we study various HTL materials like $CuSbS_2$, CuI, CuSCN, Cu_2O, NiO, and P_3HT. We see from Table VI. that $CuSbS_2$ outperforms the other HTL materials having highest V_{oc}(1.476 V), J_{sc}(14.144 mA cm^{-2}),FF(77.53%) and PCE of 16.19%. The same can be deduced from Fig.3.Where Fig. 3a. shows that using $CuSbS_2$ as HTL had highest power convergence efficiency, Fig. 3b. shows the quantum efficiency of various HTLs and $CuSbS_2$ has the highest quantum efficiency when compared to other HTLs, Fig. 3c. shows the energy band diagram of all the HTLs and Fig. 3d. shows the comparison of the J_{sc}-V characteristics of different HTLs and we can observe that $CuSbS_2$ has the highest J_{sc} and V_{oc} among other HTLs. Considering the quantum efficiency and J_{sc}- V characteristics it was decided to have $CuSbS_2$ as the HTL.

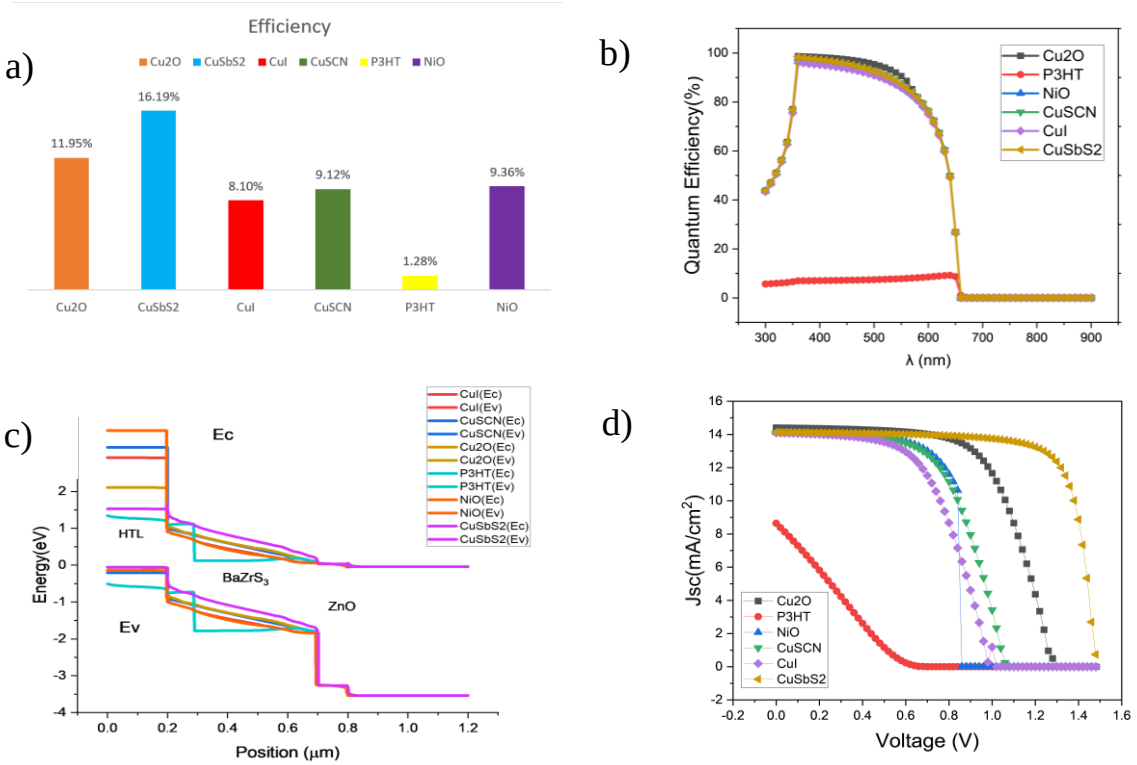

Fig. 3. Plot of different HTL on C-PSC: a) efficiency of C-PSC, b) Quantum Efficiency, c) Energy band diagram of all HTL, and d) J_{sc}–V characteristics.

Table VI Impact of different HTL on C-PSC device.

HTL	V_{oc}[V]	J_{sc} [mA cm^{-2}]	FF [%]	PCE [%]
$CuSbS_2$	1.476	14.144	77.53	16.19
CuI	0.983	14.091	58.42	8.10
CuSCN	1.056	14.116	61.13	9.12
Cu_2O	1.273	14.411	65.09	11.95
P_3HT	0.669	8.642	22.05	1.28
NiO	1.254	14.12	52.82	9.36

C. Influence of Interface Defects on CuSbS2/Absorber and ZnO/Absorber

The interface layers have a large effect on the performance of solar cell. IL1 is the interface layer between HTL and absorber, and IL2 is the interface between the ETL and absorber. To determine the effect of interface density, we vary the densities between 10^9 and 10^{15}. In the case of IL1, we see that the PCE is not changing much with the increase in defect density whereas for IL2 PCE is decreasing rapidly with an increase in defect density. In the below Fig. 4, the variation of interface defect density of ZnO/absorber is shown. The defect density of IL2 affects cell function more than that of IL1. The reason for this is that more electron-hole pairs are produced at IL2 than at IL1, which leads to a higher rate of recombination because of the excess carrier density. Our simulated results show that the higher PSC performance can be achieved with defect densities of IL1 and IL2 less than 10^{13} cm^{-3}

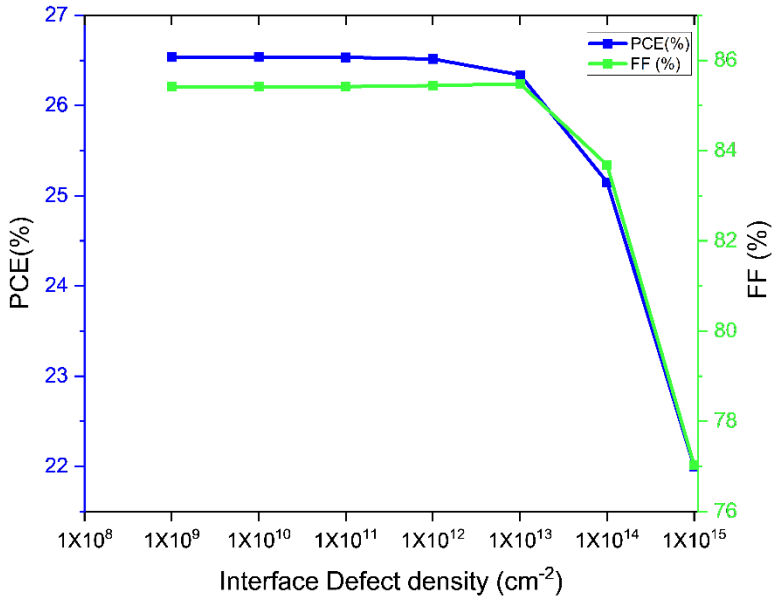

Fig. 4. Effect of interface defects: ETL/perovskite.

D. Consequence of Varying the Thickness and Defect Density of $BaZrS_3$

The performance of the device is typically substantially influenced by the absorber layer's thickness. We know that when the thickness of the absorber increases, photon absorption increases and greater charge carrier creation follows. To increase the device efficiency, we understand the impact of varying the thickness. We altered the thickness of the chalcogenide absorber from 30 nm to 1500 nm. The effect of varying thickness of the absorber layer on different electrical properties of the device with is shown in Fig. 5. We observe that the PCE dramatically increases from 10% to 23% as the thickness rises from 100nm to 500nm. After that, the rate of increase in efficiency does not change rapidly If the thickness of the absorber layer exceeds charge carrier diffusion length (ideal limit), then the probability of recombination within a layer increases. This limitation is related to the defect/trap density. From the Fig. 5. we can also observe that the PCE of the device becomes almost constant after the thickness of 1500nm, so the thickness was fixed at 1500nm for further optimization of the PSC. The thickness of 1500nm is validated from [15]

..

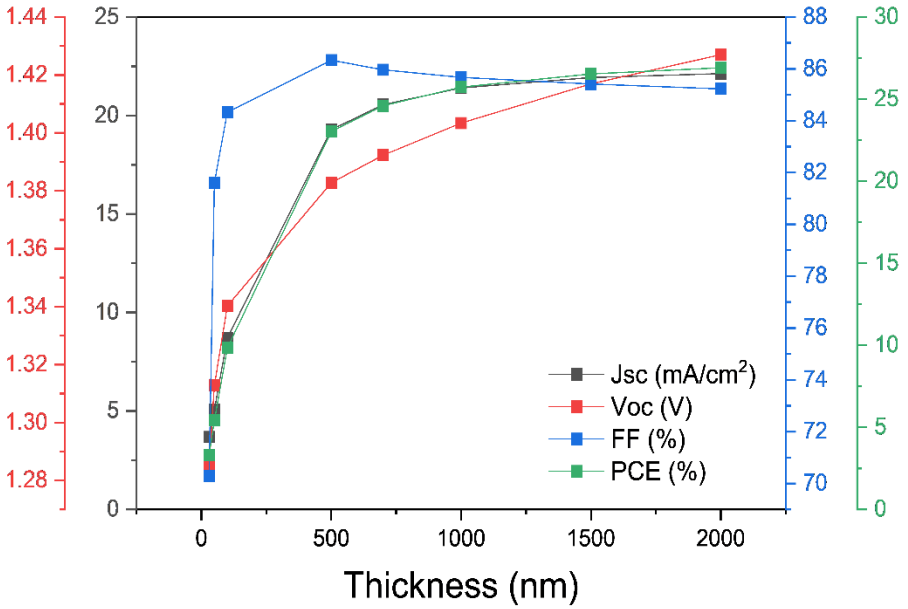

Fig. 5. Effect of the change in thickness of $BaZrS_3$

.

The performance of the device is also highly dependent on the defect density of the absorber, which is directly proportional to the perovskite layer's quality. Experimentally, it is discovered that defects in PSCs are present at the interface or surface because of uncoordinated atoms, dangling bonds [37],dislocation on the film surface, the sublimation of organic molecules during the thermal annealing process, the absence of stoichiometric compositions at the surfaces of grains, and other factors. Additionally, bulk defects like Schottky, Frenkel and intrinsic point defects (such as interstitial and vacancy defect) have a significant impact on perovskite properties [38,39]. During the collection of photo-generated charge carriers a lot of charge carriers could be lost in the case of a subpar absorber layer, which would affect device performance. Generally, the diffusion length and charge carrier lifespan are influenced by increasing defect density, resulting in larger recombination problems [40,41]. The effect of CPs absorber defect density (N_t) on the device PV characteristics was therefore extensively examined in this section while shifting the values from 1×10^{10} cm^{-3} to 1×10^{18} cm^{-3} as shown in Fig. 6. It can be observed that there is not much change in PCE when N_t is in the range of 1×10^{10} cm^{-3} to 1×10^{14} cm^{-3}. Then it gradually decreases to below

5% as the defect density increases. The diffusion lengths of holes and electrons may be decreased when absorber defect density value is increased [42]. Because the CPs layer experiences less recombination, lower N_t values result in great device performance. To realize how the variation of the interface defect densities impacts the device PV characteristics, we will alter the Absorber/HTL and ETL/Absorber interface defect densities in the section that follows using the optimized and selected value of $N_t = 1\times10^{10}$ cm^{-3} for the absorber layer

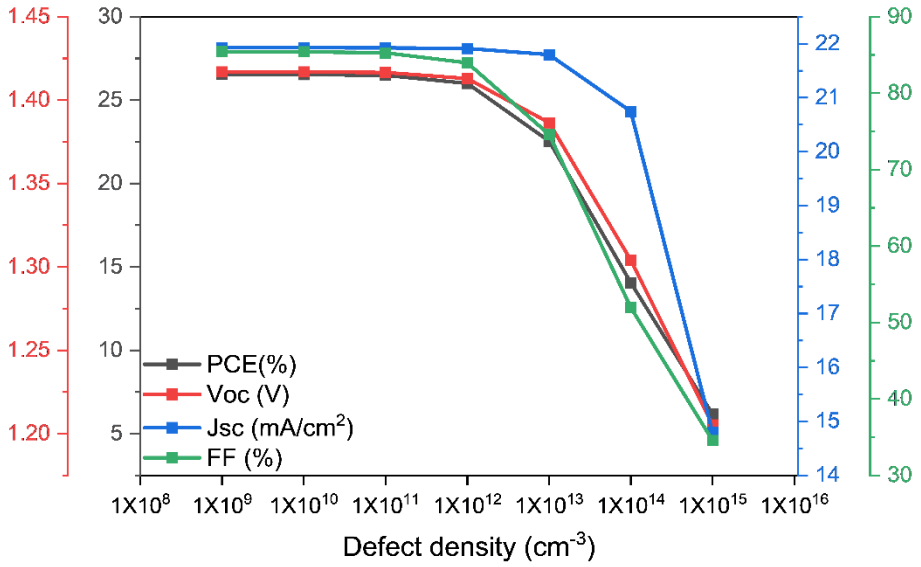

Fig. 6. Effect of change in Defect density of $BaZrS_3$

E. Discussion of proposed structure

After optimizing the reference PSC by carrying out the simulations as mentioned above, the structure of the proposed PSC is as shown in Fig. 7

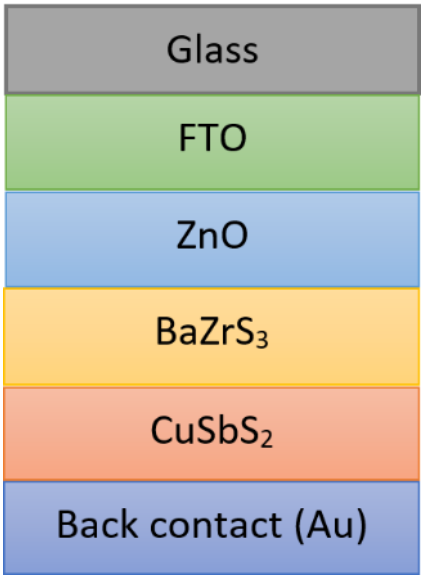

Fig. 7. Design of proposed PSC

The results obtained while optimizing the PCE structure are tabulated in Table VII. The glass base/FTO/ZnO/$BaZrS_3$/$CuSbS_2$/Au structure has a PCE of 26.54%. The findings of this paper prove

that by using $CuSbS_2$ as HTL and ZnO as ETL we arrive at a more efficient PSC than the reference PSC [17] as shown in the Table VIII.

Table VII Final results of the proposed PSC

Parameters	Optimal layers/values
ETL Material	ZnO
HTL Material	$CuSbS_2$
Absorber layer thickness	1500nm
Absorber layer defect density	10^{10}
Absorber layer bandgap	1.7eV
ETL thickness	30nm
HTL thickness	50nm
ETL defect density	10^{13}
HTL defect density	10^{14}
Interface defect density	IL1-10^{10}
	IL2-10^{10}
Metalwork function	5.4eV

Table VIII Comparison of reference PSC with the proposed PSC

Device Structure	V_{oc}[V]	J_{sc} [mA cm^{-2}]	FF [%]	PCE [%]
FTO/TiO_2/$BaZrS_3$/Cu_2O/Au (Reference[17])	1.16	12.24	87.13	12.42
FTO/ZnO/$BaZrS_3$/$CuSbS_2$/Au (Proposed)	1.4169	21.925	85.41	26.54

4. Performance analysis of the proposed Chalcogenide-PSC Device.

In the above sections we have discussed the device optimization. Below we discuss the performance of the proposed PSC Device in light of various parameters.

A. Generation and Recombination Rate

The impact of carrier generation and recombination in the C-PSC device is graphically represented in Fig. 8. According to the figure, there is a higher generation and recombination rate in the $CuSbS_2$ region than in the ZnO region, while we see an increase in the absorber region. The plot unequivocally demonstrates that the J_{sc} of the photovoltaic device is greatly increased by the addition of $CuSbS_2$ to the structure. This is because there is a higher generation rate than recombination rate in the $CuSbS_2$ region and in the $CuSbS_2$/Absorber region. The device's effectiveness consequently rises quickly.

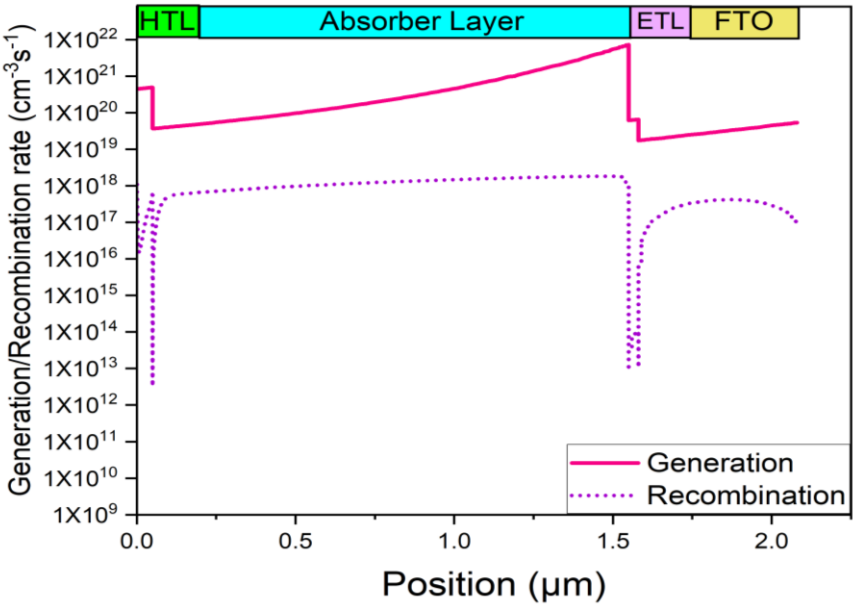

Fig. 8. Analysis of generation and recombination rate on C-PSC.

B. Carrier density Analysis

The suggested C-PSC device's carrier density is represented graphically in Fig. 9. The figure shows that holes (p) and electrons (n) migrate to their respective contacts inside the perovskite region, specifically, holes travel to the $CuSbS_2$ region and electrons travel to the ZnO region. Electron density and hole density are equivalent in the perovskite region

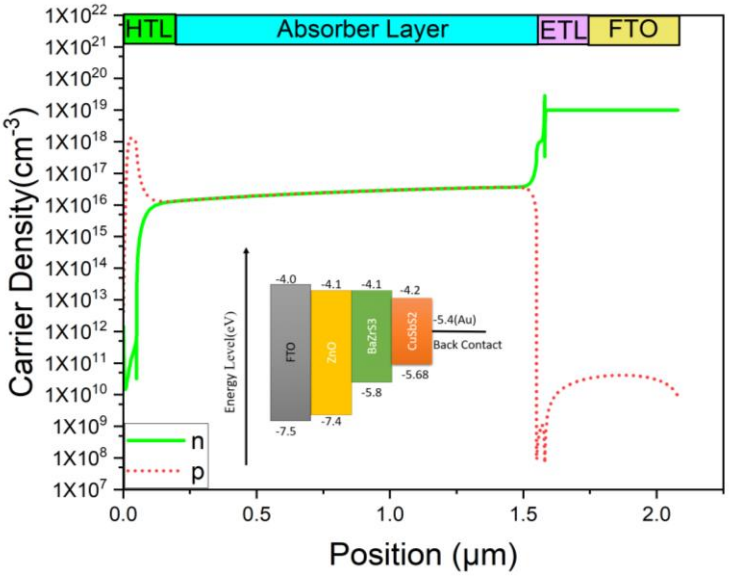

Fig. 9. Carrier density and the Energy band diagram of proposed C-PSC device.

C. Comparing the Performance of the Optimized and Unoptimized Chalcogenide-PSC

A simulation was run using ZnO as the electron transport layer's material, $CuSbS_2$ as the hole transport layer's material, the absorber layer, and FTO as the input layers. The solar cell has a PCE of 16.19 %, as shown in Table IX. A unique combination of FTO/ZnO/$BaZrS_3$/$CuSbS_2$/Au was

accomplished by optimizing the $BaZrS_3$ layer's thickness, the HTL and ETL's thickness and defects, as well as the $BaZrS_3$ layer's interface defects with the HTL and ETL and the cell's series and shunt resistance. As a consequence of this combination, the device's PCE greatly boosted. As shown in Fig. 10, the optimized solar cell reached current density of 21.925 mA/cm^2 and a Voc of 1.4 V. The optimized PSC offers a 10.45% increase in efficiency over a solar cell that has not been optimized

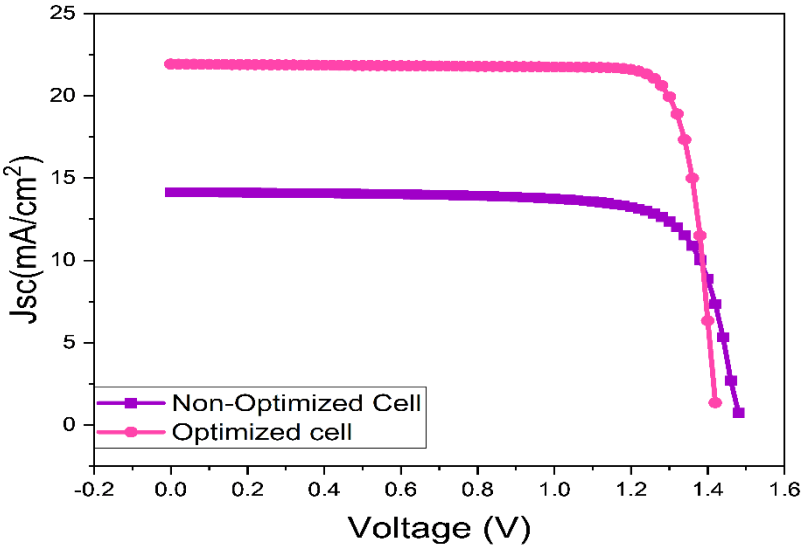

Fig. 10. J_{sc}–V characteristics of the optimized and non-optimized Chalcogenide-based PSC device.

A photovoltaic cell's QE provides information on how much current it will generate in response to photons of a particular wavelength. Fig. 11 shows the QE of the proposed C-PSC device both in its unoptimized and optimized states. The graphical study shows that a device with optimization absorbs more photons than a device without optimization. By the graphical analysis, we can see that for the non-Optimized cell the Quantum efficiency starts decreasing exponentially after the wavelength becomes 400nm. But for the Optimized cell, the Quantum efficiency is 100% from 350nm to 700nm, which is quite a lot of improvement from the non-Optimized cell as indicated in Table IX. The current density in the solar cell increases from 14.144 to 21.925 mA/cm^2. This results in an increase of the device's efficiency to 26.54 %

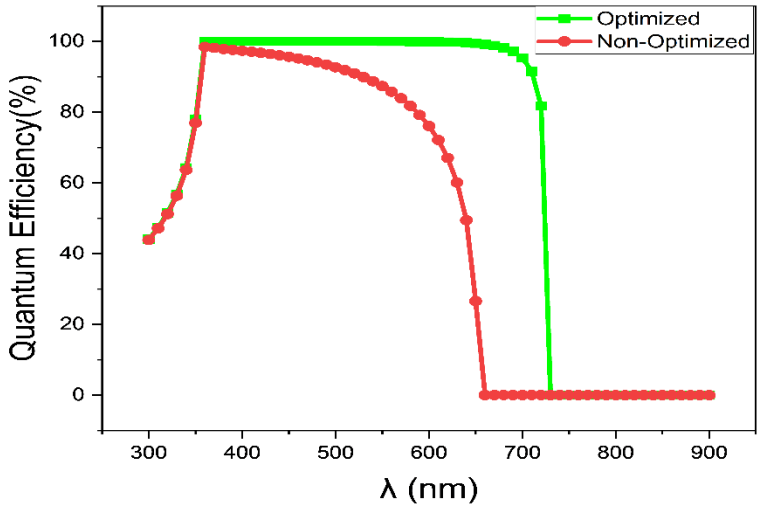

Fig. 11. QE analysis on Non-optimized and optimized C-PSC.

Table IX Comparison of reference PSC with the proposed PSC

PSC/Parameters	V_{oc}[V]	J_{sc} [mA cm^{-2}]	FF [%]	PCE [%]
Nonoptimized solar cell	1.4761	14.144	77.53	16.19
Optimized solar cell	1.4169	21.925	85.41	26.54

5. Conclusion

In this communication, we presented numerical simulation of a novel lead-free Perovskite Solar Cell based in $BaZrS_3$ using SCAPS-1D. Various ETL and HTL Combinations were considered from the point of view of efficiency. We optimized the thickness, bandgap and defect density of the absorber layer to obtain a better power conversion efficiency of 26.54%. Whereas in the non-optimized PSC had PCE of 16.19%. Then we checked the performance of the proposed PSC on various benchmarks like generation and recombination analysis of generated carrier, their density and current voltage performance.

6. References

[1] Singh NK, Agarwal A, Kanumuri T (2022) Performance Enhancement of Environmental Friendly Ge-Based Perovskite Solar Cell with Zn3P2 and SnS2 as Charge Transport Layer Materials. Energy Technology 10

[2] Green M, Dunlop E, Hohl-Ebinger J, et al (2021) Solar cell efficiency tables (version 57). Progress in Photovoltaics: Research and Applications 29:3–15

[3] Farhat M, Baloch AAB, Rashkeev SN, et al (2020) Bifacial Schottky-Junction Plasmonic-Based Solar Cell. Energy Technology 8:.

[4] Zhao P, Su J, Lin Z, et al (2020) All-Inorganic CsPbIxBr3−x Perovskite Solar Cells: Crystal Anisotropy Effect. Adv Theory Simul 3:2000055.

[5] Wang M, Wang W, Ma B, et al (2021) Lead-Free Perovskite Materials for Solar Cells. Nano-Micro Letters 2021 13:1 13:1–36.

[6] Tiwari D, Hutter OS, Longo G (2021) Chalcogenide perovskites for photovoltaics: current status and prospects. Journal of Physics: Energy 3:034010.

[7] Yu Z, Wei X, Zheng Y, et al (2021) Chalcogenide perovskite BaZrS3 thin-film electronic and optoelectronic devices by low temperature processing. Nano Energy 85:105959.

[8] Wei X, Hui H, Zhao C, et al (2020) Realization of BaZrS3 chalcogenide perovskite thin films for optoelectronics. Nano Energy 68:104317

[9] Márquez JA, Rusu M, Hempel H, et al (2021) BaZrS3Chalcogenide Perovskite Thin Films by H2S Sulfurization of Oxide Precursors. Journal of Physical Chemistry Letters 12:2148–2153.

[10] Comparotto C, Davydova A, Ericson T, et al (2020) Chalcogenide Perovskite BaZrS3: Thin Film Growth by Sputtering and Rapid Thermal Processing. ACS Appl Energy Mater 3:2762–2770.

[11] Nishigaki Y, Nagai T, Nishiwaki M, et al (2020) Extraordinary Strong Band-Edge Absorption in Distorted Chalcogenide Perovskites. Solar RRL 4:1900555

[12] Sharma S, Ward Z, Bhimani K, et al (2021) Bandgap Tuning in BaZrS3Perovskite Thin Films. ACS Appl Electron Mater 3:3306–3312.

[13] Adjogri SJ, Meyer EL (2021) Chalcogenide Perovskites and Perovskite-Based Chalcohalide as Photoabsorbers: A Study of Their Properties, and Potential Photovoltaic Applications. Materials 14:7857

[14] Burgelman M, Nollet P, Degrave S (2000) Modelling polycrystalline semiconductor solar cells. Thin Solid Films 361–362:527–532.

[15] Meng W, Saparov B, Hong F, et al (2016) Alloying and Defect Control within Chalcogenide Perovskites for Optimized Photovoltaic Application. Chemistry of Materials 28:821–829.

[16] Ravi VK, Yu SH, Rajput PK, et al (2021) Colloidal BaZrS3chalcogenide perovskite nanocrystals for thin film device fabrication. Nanoscale 13:1616–1623.

[17] Karthick S, Velumani S, Bouclé J (2022) Chalcogenide BaZrS3 perovskite solar cells: A numerical simulation and analysis using SCAPS-1D. Opt Mater (Amst) 126

[18] Azri F, Meftah A, Sengouga N, Meftah A (2019) Electron and hole transport layers optimization by numerical simulation of a perovskite solar cell. Solar Energy 181:372–378.

[19] Lakhdar N, Hima A (2020) Electron transport material effect on performance of perovskite solar cells based on CH3NH3GeI3. Opt Mater (Amst) 99:109517.

[20] Chatterjee S, Pal AJ (2016) Introducing Cu2O thin films as a hole-transport layer in efficient

planar perovskite solar cell structures. Journal of Physical Chemistry C 120:1428–1437.

[21] Liu X, Yan K, Tan D, et al (2018) Solvent engineering improves efficiency of lead-free tin-based hybrid perovskite solar cells beyond 9%. ACS Energy Lett 3:2701–2707.

[22] Guo Y, Jiang J, Zuo S, et al (2018) RF sputtered CdS films as independent or buffered electron transport layer for efficient planar perovskite solar cell. Solar Energy Materials and Solar Cells 178:186–192.

[23] Shivesh K, Alam I, Kushwaha AK, et al Investigating the theoretical performance of Cs 2 TiBr 6-based perovskite solar cell with La-doped BaSnO 3 and CuSbS 2 as the charge transport layers

[24] Teimouri R, Mohammadpour R (2018) Potential application of CuSbS2 as the hole transport material in perovskite solar cell: A simulation study. Superlattices Microstruct 118:116–122.

[25] Gharibzadeh S, Nejand BA, Moshaii A, et al (2016) Two-step physical deposition of a compact cui hole-transport layer and the formation of an interfacial species in perovskite solar cells. ChemSusChem 9:1929–1937.

[26] Qin P, Tanaka S, Ito S, et al (2014) Inorganic hole conductor-based lead halide perovskite solar cells with 12.4% conversion efficiency. Nature Communications 2014 5:1 5:1–6.

[27] Jung M, Kim YC, Jeon NJ, et al (2016) Thermal Stability of CuSCN Hole Conductor-Based Perovskite Solar Cells. ChemSusChem 9:2592–2596

[28] Karthick S, Nwakanma OM, Mercyrani B, et al (2021) Efficient 2T CsKPb(IBr)3—Tin Incorporated Narrow Bandgap Perovskite Tandem Solar Cells: A Numerical Study with Current Matching Conditions. Adv Theory Simul 4:2100121.

[29] Bhattarai S, Pandey R, Madan J, et al (2022) Investigation of Carrier Transport Materials for Performance Assessment of Lead-Free Perovskite Solar Cells. IEEE Trans Electron Devices 69:3217–3224.

[30] Subbiah AS, Halder A, Ghosh S, et al (2014) Inorganic hole conducting layers for perovskite-based solar cells. Journal of Physical Chemistry Letters 5:1748–1753.

[31] Devi C, Mehra R (2019) Device simulation of lead-free MASnI3 solar cell with CuSbS2 (copper antimony sulfide). J Mater Sci 54:5615–5624.

[32] Christians JA, Fung RCM, Kamat P v. (2014) An Inorganic Hole Conductor for Organo-Lead Halide Perovskite Solar Cells. Improved Hole Conductivity with Copper Iodide. J Am Chem Soc 136:758–764.

[33] Karthick S, Bouclé J, Velumani S (2021) Effect of bismuth iodide (BiI3) interfacial layer with different HTL's in FAPI based perovskite solar cell – SCAPS – 1D study. Solar Energy 218:157–168.

[34] Gan Y, Bi X, Liu Y, et al (2020) Numerical Investigation Energy Conversion Performance of Tin-Based Perovskite Solar Cells Using Cell Capacitance Simulator. Energies 2020, Vol 13, Page 5907 13:5907.

[35] Minemoto T, Murata M (2014) Impact of work function of back contact of perovskite solar cells without hole transport material analyzed by device simulation. Current Applied Physics 14:1428–1433

[36] Verschraegen J, Burgelman M (2007) Numerical modeling of intra-band tunneling for heterojunction solar cells in scaps. Thin Solid Films 515:6276–6279.

[37] Wang F, Bai S, Tress W, et al (2018) Defects engineering for high-performance perovskite solar cells. npj Flexible Electronics 2018 2:1 2:1–14.

[38] Maiti A, Chatterjee S, Peedikakkandy L, Pal AJ (2020) Defects and Their Passivation in Hybrid Halide Perovskites toward Solar Cell Applications. Solar RRL 4:2000505.

[39] Ball JM, Petrozza A, Ball JM, Petrozza A (2016) Defects in perovskite-halides and their effects in solar cells. NatEn 1:16149.

[40] Singh N, Agarwal A, Agarwal M (2020) Numerical simulation of highly efficient lead-free all-perovskite tandem solar cell. Solar Energy 208:399–410.

[41] Zekry A, Shaker A, Salem M (2018) Solar Cells and Arrays: Principles, Analysis, and Design. Advances in Renewable Energies and Power Technologies 1:3–56.

[42] Et-taya L, Ouslimane T, Benami A (2020) Numerical analysis of earth-abundant Cu2ZnSn(SxSe1-x)4 solar cells based on Spectroscopic Ellipsometry results by using SCAPS-1D. Solar Energy 201:827–835